31st Congress of the International Council of the Aeronautical Sciences

Belo Horizonte, Brazil; September 09-14, 2018

WIND TUNNEL EXPERIMENTS WITH LOCAL ACTIVE FLOW CONTROL FOR AIRCRAFT TOWARDS FUTURE FLIGHT TESTING

Vlad Ciobaca*, Bruno Stefes, Anton de Bruin***, Matthias Bauer*****, Philipp Schlösser******, Arnoud de Blécourt***, Niko Bier*, Junnai Zhai*******, Michael Meyer**, Jochen Wild***

***Deutsches Zentrum für Luft und Raumfahrt, DLR, Braunschweig, Germany,**
****Airbus Operations GmbH, Bremen, Germany,**
*****NLR-Netherlands Aerospace Center, Marknesse, The Netherlands,**
******Airbus Defence and Space GmbH, Munich, Germany,**
*******NAVASTO GmbH, Berlin, Germany,**
********DNW-KKK, Cologne, Germany.**

Keywords: *transport aircraft, active flow control, pylon/wing junction, high-lift*

Abstract

A high Reynolds number wind tunnel test with a single aisle transport aircraft model at low speed cryogenic conditions is addressing the challenges to apply local active flow control technologies to delay the wing stall at high-lift conditions and enable the close-coupling of UHBR engines. The study considers flow control technologies to be matured towards a future flight test with DLR's ATRA test aircraft. The research focuses on studying the impact of a so-called slat cutout inboard of the under-wing mounted engine and verifies the aerodynamic benefits of flow control systems towards the flight test.

1. Introduction

One way of improving the tube-wing aircraft configuration is to integrate modern and efficient engines. For passenger aircraft a closely-coupled Very High Bypass Ratio (VHBR) turbofan engine and a backward swept wing is currently becoming state-of-the art and research and development regarding the engine integration is considering even larger engines of the Ultra High Bypass Ratio (UHBR) category for further benefits in fuel saving and environmental protection.

Already for todays' VHBR engines the integration under the wing of current conventional aircraft (e.g. - of single-aisle a/c-Airbus A320neo, Boeing 737MAX, Embraer E-Jet E2) is challenging, but becomes even more so when under-the-wing mounted UHBR engines are considered.

For the cruise flight the mounting of a UHBR can be well designed for minimum drag and low direct operating cost (DOC), but for the low speed flight phases the challenges reflect the impact of closely-coupled engines on the design of high-lift devices. The close-coupling of the UHBRs is driven by multiple constraints such as maintaining the ground clearance for engines, saving weight for an optimized pylon structure and/or improving aerodynamics at cruise flight (Lange [1]). Furthermore the leading edge high-lift device needs to be shortened due to the larger engine, causing high-lift degradation during landing. This reduces both the maximum angle of attack and the maximum lift coefficient, which results in higher landing speeds, longer landing fields, or will reduce payload and/or range due to the take-off weight limitation. The current aircraft show the use of state-of-the-art technologies (e.g. nacelle strakes, and small Krüger on Boeing787) to partially alleviate these effects. Recent research performed in Europe (Lengers[2], Fricke et al.[3], Meyer and Wildscheck [4], Bauer et al.[5]) has

shown that the degradation during landing is partially recovered by means of AFC through energizing the flow with fluidic jets.

The application of local Active Flow Control (AFC) at the unprotected wing leading edge resulting at the junction between a closely-coupled UHBR engine and a swept wing is the focus of this study. The motivation is twofold. On the one hand UHBR engines with very high bypass ratio and lower Fan Pressure Ratios (FPR) have a considerable potential for ecologic and economic benefit in civil aviation [6]. On the other hand, the integration becomes even more challenging when novel aircraft configurations are considered.

The objective of this work is to use the lessons learned during several decades of research on AFC for global aerodynamic enhancements, together with very recent work on local AFC towards the implementation of AFC technologies aiming for the delay of flow separation during flight.

This paper will report on the general approach for this technology, will include numerical results, and will provide details on recent results of the high-Reynolds number wind tunnel testing with AFC by means of fluidic actuation with a well-detailed high-lift model.

2. Methods and Tools

The approach is based on assimilating existing studies for separation control for a fast development of the AFC technologies through numerical and experimental studies. We mention first few recent background researches and present afterwards the methods and tools used for our studies which include high fidelity RANS simulations, actuator development and wind tunnel testing at large Reynolds numbers in a low speed cryogenic facility.

2.1 Historical Background

Using passive and active flow control devices to delay the local wing stall towards larger angles of attack in the absence of local high-lift devices (e.g. slat, Krüger) was established as a well-documented practice both for studies on airfoils and for complex high-lift wing body configurations (Lachmann [7] Joslin and Miller [8]). Active systems applied on unprotected leading edges for airfoils have proved effective, but classical high-lift slat devices remain usually superior with respect to the maximum lift produced at a wing section (Smith [9]). The application for a local active flow control, where only a limited span of a wing has an unprotected leading edge, poses a different challenge. In a way the problem is similar to the application of nacelle strakes for increasing maximum lift at typical landing configurations or passive devices (e.g. fences) applied at the wing tip for delaying the local flow separation. Here, the main scope of the AFC application remains the local flow separation control for allowing some extension of the flight envelope and typically the interaction with a vortex-dominant flow.

A recent low speed and low Reynolds number wind tunnel test with a half-model transport aircraft configuration and the corresponding aerodynamic evaluation for tangential blowing flow control towards the application at the pylon/wing junction was reported by Lengers [2] *5.6%* increment for maximum lift and in the order on *2.5°* for maximum angle are reported. Experimental research for the application of vortex generator jets and fluidic actuators to delay the flow separation of outer wings was reported in Ciobaca et al [10]. Gains in the order of *2°* were achieved at moderate *Re* and typical aircraft (A/C) low speed conditions of Mach *Ma=0.2*. Applying local flow control was continued for the wing tip region in a European framework as reported by Rosenblum et al. [11] with a good knowledge gain based on different numerical methods and tools, for the assessment of constant blowing, pulsed actuation and synthetic jets with a reference wing configuration for a long range aircraft. Amiryants et al. [12] report the continuous effort for the application on the pylon/ wing junction including large Reynolds number testing with a model well-suited for the system tests of actuation. Local flow separation control was well documented in the wind tunnel tests at Tsagi T-101 through tufts visualization and balance data with a well monitored fluidic

actuation system developed towards the A/C level. The results are very promising towards the application for UHBR configurations.

With the scope to further mature the AFC technologies for the pylon/wing junction both testing at large Re with a half-wing model of a relevant configuration and preparing the systems towards a demonstrator are of interest. The ATRA was identified as one possible demonstrator for the study of AFC on unprotected leading edges (LEs). The hypothesis is that a shorter inboard slat with a classical nacelle of a V2500 engine may simulate the maximum lift loss-effects of under-the-wing mounted UHBRs. In the frame of the Clean Sky 2 Joint Undertaking [13] under the European Union's Horizon 2020 research and innovation program this approach is under investigation within a collaborative work of industry (Airbus) and several research institutions.

The planned activities cover wind tunnel testing (WTT), a ground test demonstrator (GTD) and a flight test demonstrator (FTD).

This paper will focus on the analysis of wind tunnel data, and is therefore covering mainly aerodynamic aspects. However, as shown in Fig. 1, such wind tunnel test studies are strongly related to a possible flight test. The numerical environment (CFD) covers setups for AFC feasible with given structural (FEM) modifications for the wing, with limited mass-flows (pre-design of Air Supply) and with expected volumes for fluidic actuators to allow a safe operation during a flight phase demonstration. Therefore we use the cryogenic testing both for reaching the required high Reynolds number testing as well as to ensure a first test of a configuration that is targeted to be able to take-off and land.

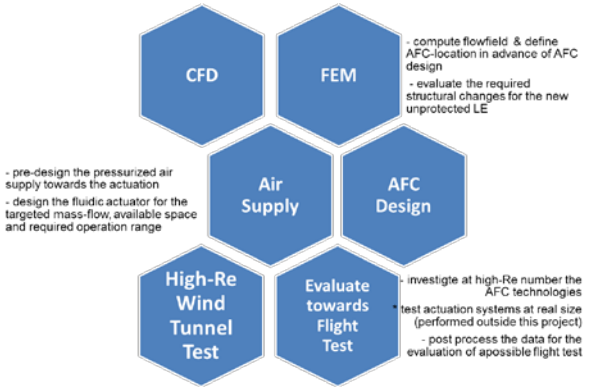

Fig. 1. Involved activities for AFC studies

2.2 Numerical Approach

The study of flow control is addressed numerically by steady and unsteady RANS simulations and uses approaches reported in [14], [15] for applications of steady and unsteady flow control. The DLR TAU solver is used to compute the landing configuration of the short range a/c, a challenge by itself being the maximum lift evaluation (see Rudnik and Schwetzler [16]) in addition to the targeted AFC evaluation. The modelling of actuators is limited to simple geometries below the wing surface and the use of a transpiration boundary condition. The major target of the CFD study with the RANS simulations was to learn the most promising chordwise position (*x/c*) of the actuation slits. The unit of measure was the flow sensitivity for constant blowing. With a selected *x/c* location the application of fluidic actuators was afterwards investigated at various fixed AoAs larger than the baseline AoA-max.

The maximum lift investigations were addressed using hybrid meshes generated with the Centaur mesh generator and were computed with a central scheme and low numerical dissipation (matrix dissipation). The studies required meshes with about 80 million nodes and several weeks for running on a high-performance cluster for a steady polar simulation.

2.3 Wind Tunnel Testing

The wind tunnel test could use background high-Reynolds data (e.g. tests in DNW-KKK without slat cutout and without AFC) and the existing model [17]. The selected atmospheric low speed facility, DNW-KKK, allows for both testing at temperatures down to *100K*, and for Mach number between *0.1* and *0.3*. This results for the considered model in a chord Reynolds number of up to 10 Million. The facility supplies pressurized nitrogen at the actuator systems and can support the control of various mass-flows as shown over the previous studies (e.g. [18]). For half-model measurements the gas supply pipeline with corresponding force measuring technique for the cryogenic working environment has been developed and successfully tested (see Zhai and Vree [19]). Alternative coupling element types were analyzed that can be

configured to an airline-bridge that is very flexible compared to loaded balance though stiff enough to compensate the reaction force from the inner pressure. The airline bridge with a flexible hose type of coupling has successfully been applied during a wind tunnel test confirming its suitability for applying Active Flow Control technology in a cryogenic environment. The influence on the force measurement by the stiffness, pressure and temperature of the airline bridge designs has been shown to be negligible. The gas supply pipeline below the test section was isolated and partially heated.

The tunnel temperature is controlled by injection of liquid nitrogen in the closed loop tunnel. The test section is *2.4m x 2.4m* (width times height) and has a low turbulence level.

The forces were measured with a balance mounted below the fuselage, and the Kulite data (3 sensors in wing LE and four sensors for monitoring unsteady pressure in the AFC unit) were DC measured at *20.54 kHz* with a Viper data acquisition system. For monitoring the flow topologies tufts visualizations were made at atmospheric conditions.

2.4 Wind Tunnel Model

The HINVA high-lift model was designed as a right-hand half-model at a scale of *1:13.6*. As is common practice for high-lift half-model testing, the empennage of the real aircraft is neglected for the wind tunnel model. The model was built of high-strength aluminum. The mounted model during the previous wind tunnel testing performed in the European Transonic Windtunnel ETW is shown in Fig. 2. The focus here is on the model in the landing (FULL) configuration with *40°* deflection of the Fowler flap. The slat brackets and the de-icing pipe are scaled from the real aircraft and manufactured from steel with hollow structures. Through-flow-nacelle (TFN) is mounted under the backward swept wing and the parts of the so-called lift-improvement package (LIP) are also used for our experiments. The wing is equipped with nearly *450* pressure taps in five chordwise sections and five spanwise sections. The model is well covered with coatings for measurements: particle image velocimetry (PIV) in the field and laminar-to-turbulent transition regarding the local boundary layer.

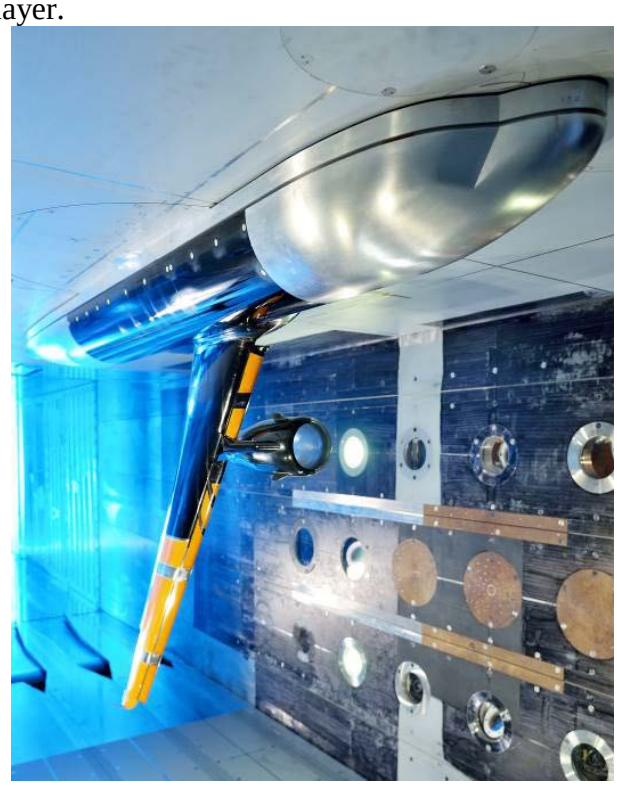

Fig. 2. HINVA model in ETW, taken with permission from [17].

Regarding the experiments reported in this publication new parts had to be designed and manufactured by NLR for the existing HINVA model, in order to resemble the ATRA configuration with shortened slat and installed AFC unit, supposed to be flight tested. The new wing LE consists of three main parts, as shown in Fig. 3. Part 3 hosts a small AFC unit, developed and installed by NAVASTO. The original position of the static pressure row (HINVA model) could not be kept due to space limitations and was shifted to inboard LE part number 1. The pressure row at the new shortened slat could be kept at original span wise position. The outboard LE part number 4, consists of a main part and a cover with three Kulite sensors mounted directly below it. Also the other Kulite sensors for monitoring the operation of the AFC unit are mounted below this cover plate, as shown in Fig. 4. Gaseous nitrogen is supplied to the AFC unit with a tube entering at wing root (item 8 in Fig. 4) and is fed through a bore across the inboard LE part and leakage free into the AFC unit. NLR also designed and manufactured an UHBR nacelle and pylon and a further shortened slat for future wind tunnel testing.

After assembly of the new model parts on the existing model, all new parts were painted black (see Fig. 5) to enable PIV measurements. After extensive checking of instrumentation the model was mounted in the DNW-KKK wind tunnel. A picture of the model preparation in the DNW-KKK model lock is shown in Fig. 6.

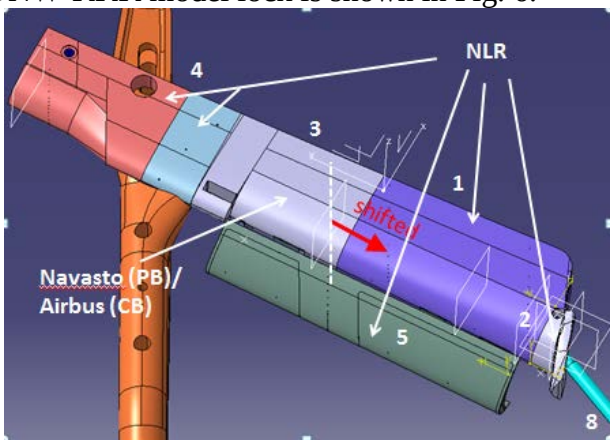

Fig. 3. New model parts for the HINVA KH-320 HA regarding the V2500 nacelle configuration

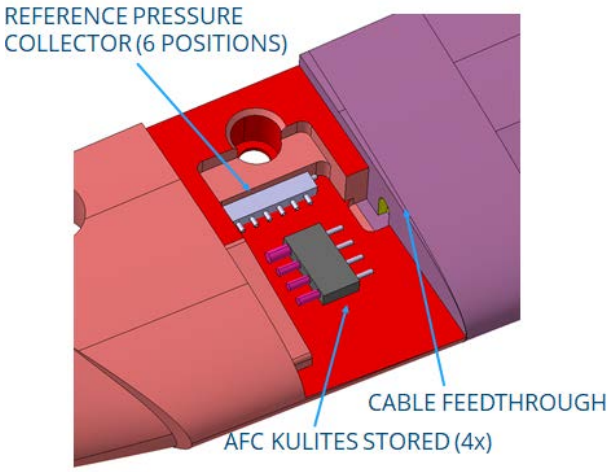

Fig. 4. Installation of the AFC Kulites

Fig. 5. Assembled model after painting

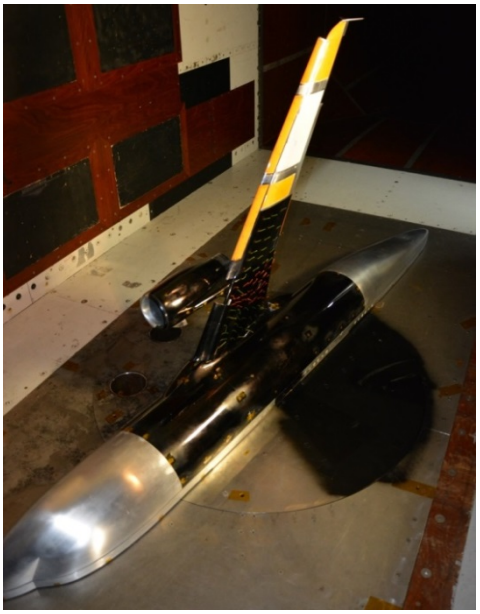

Fig. 6. HINVA High-Lift Model with slat cutout and AFC installed in DNW-KKK

2.5 Actuation System

Two types of actuation systems were developed for this test: a pulsed jet actuator (PJA) and a steady blowing actuator (SBA).

The PJA follows a two-stage approach. It combines a driving stage (or first stage) and an outlet stage (or second stage) to generate fluid pulses in an efficient manner by exploiting the effect of “fluid amplification”. The system is characterized by flow channels, which are tuned to each other to produce the desired characteristics. The outlet stage is formed by a cluster of fluidic diverter elements (also referred to as bistable switch). In each of those elements one primary jet is switched between two flow channels, each of which is connected to an outlet on the aerodynamic surface of the model wing. Switching is induced by applying a periodic, pneumatic control signal to the power jet. This pneumatic control signal is referred to as a control jet: a stream of fluid that is oriented approximately perpendicular to the main flow direction and which is much weaker than the power jet in terms of momentum and mass flow content (hence the term fluid amplification). The pneumatic control signal is generated in the driving stage, named so for its ability to imprint the switching frequency on the second stage. Within the driving stage, a feedback mechanism, analogous to the one found in resistance induced

oscillators, causes the flow to switch periodically between two branches when fluid passes through it. Each branch of the driving stage has multiple outlets, which are connected to the diverter elements of the second stage, thus providing them with the required pneumatic control signal. The internal flow topology of the actuator system is shown in Fig. 7 with the outlet stage in the front and the driving stage in the back of the image.

A total of 6 outlet slits were integrated in the model wing surfaces oriented in parallel to the leading edge. By design, the entire system covered a total span of approximately 20mm. During the installation of the AFC system in the model wing the two most outboard slits needed to be partially closed, which resulted in a steady state jet at these two locations. The AFC system was validated and calibrated based on numerical data and in experiments. Fig. 8 shows the output signal of the AFC system in terms of total pressure at one slit.

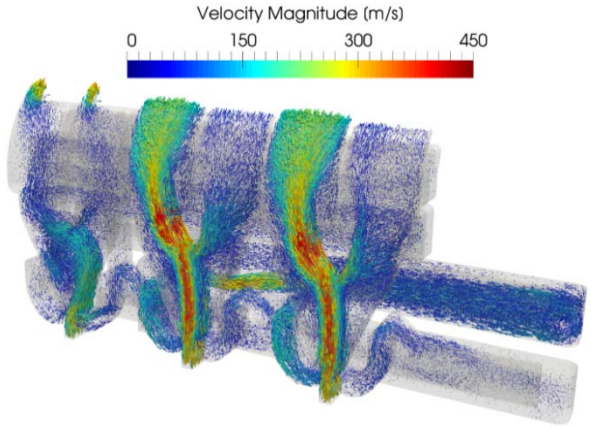

Fig. 7. Simulation of the PJA device with reduced outlet cross-section at the most outboard element

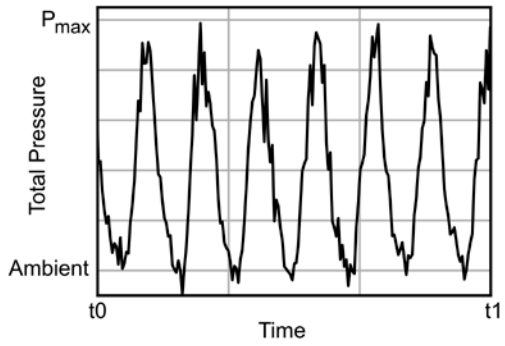

Fig. 8. Output signal of PJA meassured with a Kulite pressure transducer at the most inboard slit.

The pulsed jet actuator is calibrated based on experimental data, which provides the shape of the pulsed jet in time, the recorded mass flow rates used in the experiments, measured with a mass flow meter and the temperature data at the outlet from simulations.

The SBA system is less complex than the PJA. It produces a continuous jet that is usually ejected through one single slot in the wing's upper surface. The entirety of this actuator's internal design aims at providing a homogeneous jet velocity along the slot's span. This is done by using an inner plenum and an outer plenum, which are connected via several (in-line or staggered) small holes. This setup, also referred to as a Piccolo tube, is commonly used in aircraft de-icing systems. The holes between the plena are designed to exhibit sonic flow conditions at design point. The homogeneity is then reached by the effect, that the flow through each hole is limited (assuming a common density and pressure of the fluid in the inner plenum), because choking at the holes will occur and the excess fluid is forced to pass through other holes with less flow rate through them. The jets through the holes then impinge on the wall of the outer plenum and the fluid exits the slot in the surface with a homogeneous velocity profile along the span. Again, the actuator system was calibrated using numerical and experimental tools.

The two actuator systems manufactured for the wind tunnel test are depicted in Fig. 9. Six discrete slits with a 30° inclination against the local surface are noticed for the PJA unit. The SBA consists of a single tangential slit and the manufactured insert has the same size as the PJA unit for mounting in the leading edge part 3 depicted in Fig. 3.

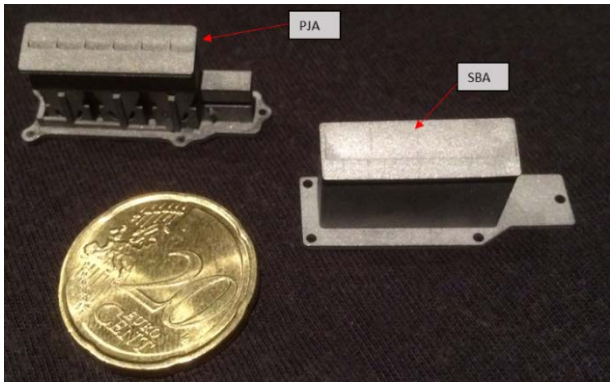

Fig. 9 Image showing the PJA and the SBA system 3D printed from stainless steel.

3. Definition of Flow Control with Constraints

The AFC application towards the demonstrator is limited by the structural and system constraints that would allow for a flight test. The hot pressurized air is supplied from the engine, a safety valve is mounted close to the actuation system and the spanwise extend of the slat cutout is in the order on *10%* of the inboard slat. Fig. 10 and Fig. 11 show the region of actuation relative to the reference high-lift wing.
With the given constraints the selected actuation system includes six slits of aspect ratio of about seven, i.e. three fluidic actuators, positioned parallel to the wing leading edge. The actuation was shown by many studies to be most effective when positioned close to region of large unsteadiness, or in other words there is to be expected a good efficiency close to the separation line/region. The actuation was investigated from 1% x/c to *7.5% x/c* in the "design box" to interact, as later shown in Fig. 12, with both, a local flow separation at the wing leading edge (LE), and with a wing flow recirculation moving from the trailing edge (TE) upstream when the incidence is increased.

3.1 General Constraints

The spanwise extend of the slat cutout is limited at the wing inboard side by the position of the slat track and by the closing rib at the wing outboard side near to the pylon. The demand to reduce the overall modifications of the flight test aircraft during the AFC installation prevented the extension of the AFC system into outboard direction. Therefore the AFC system was not extended also into the wing LE downstream of the pylon.

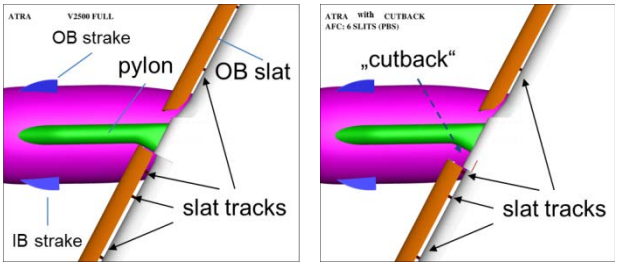

a) without cutback b) with cutback and AFC

Fig. 10. CAD view of a short range aircraft at landing with an inboard slat cutout and active flow control

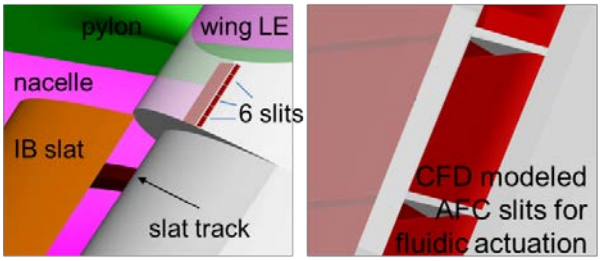

Fig. 11. Details of the modeled AFC slits (for a right wing)

The bleed air off-take form the engine is not considered being detrimental on the engine performance during landing. However, during take-off and climb, the amount of bleed air has a strong negative impact on the engine performance. In consequence, the amount of bleed-air to be used for the AFC was limited to an order of *1kg/s*. In addition there is a strong request to increase the efficiency of the PJA, reducing to a minimum the net mass flow for the PJA while assuring the effectivity of flow separation control.

3.2 CFD results

Fig. 12 shows a comparison of the skin friction lines and the streamlines through the most relevant vortices (nacelle, pylon, strake(s), and slat edge – vortices) for the same high angle of attack below maximum lift. The baseline configuration without AFC is depicted in the Fig. 12a.

Fig. 12b presents the computed result with actuation. Here the actuation in CFD is only represented by constant blowing through pulsed blowing slits, i.e. a constant uniform jet through actuators inclined with 30° compared to the local surface. The differences between the configurations are generally small on a global level. However, some notable differences are visible. Mainly this concerns spanwise shifts of the trajectories of the side edge vortex of the AFC-module (red streamlines) and the slat cove vortex (green streamlines). Especially the latter influences the separation behaviour of the flow near the main wing trailing edge and thus, the achievable maximum lift.

Fig. 13 shows the lift curves over the incidence of the aircraft for baseline and with flow control. A cutout of the inboard slat for the landing full configuration at *Ma=0.195* and at

flight Re_c of *14 m*illion resulted in a notable decrease of maximum lift in comparison with a conventional slat length. The flow breakdown occurs downstream of the unprotected LE. It is expected to regain partially this maximum lift loss by the larger surface of the UHBR engine compared to the V2500 configuration. Therefore a full recovery just due to AFC remains out of the scope of our research, and gains in the order of *10* to *50%* are of interest. Various flow control setups showed (see Fig. 13) a potential to recover up to an order on 30% of the lift loss and *1.5°* for maximum angle.

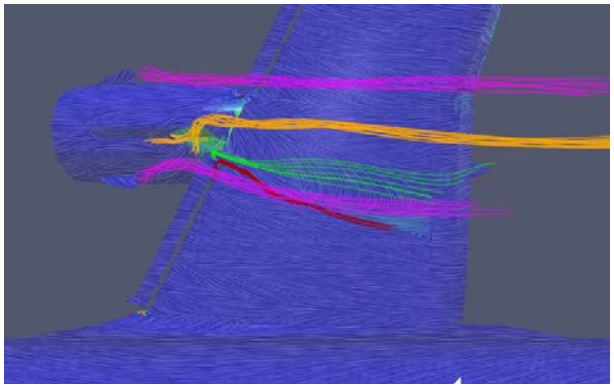

a) without AFC

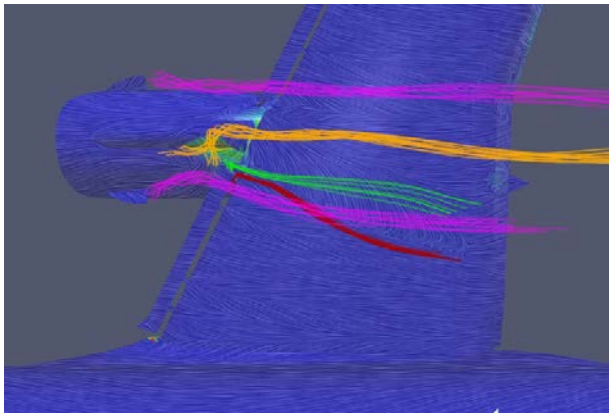

b) with AFC

Fig. 12. Numerical simulation at large incidence for a SRA aircraft at landing with an inboard slat cutout

In general, summarizing the results, close to maximum lift the initial flow recirculation at the unprotected wing LE and at main wing TE are visible (Fig. 12a). With the further increase of incidence the separation extends in spanwise direction leading to local wing stall (not shown). With flow control the local flow separation at the wing LE is reduced, and the wing stall is delayed. The *5% x/c* was found to be most promising location for AFC, such that both maximum alpha and maximum lift may be improved. The retarded boundary layer is filled by the addition of energy by AFC. Moreover, the analysis suggested that the interaction of the *30°* inclined actuation with the slat-edge vortex stabilizes the flow.

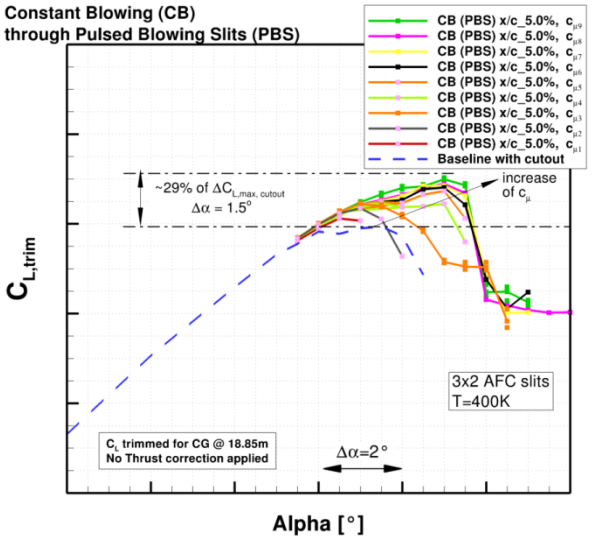

Fig. 13. Lift curves for the baseline, the reference flow with cutback and for different jet velocities with the constant blowing actuation at x/c=5% ($c_{\mu 1}<c_{\mu 2}<\ldots<c_{\mu 9}$)

4. Results

This chapter discusses the results gained during the wind tunnel testing. First the baseline (without AFC and with slat cutout) is analyzed in section 4.1. Afterwards the results with AFC are depicted in section 4.2. For the sake of clarity, in this section, all lift curves and pressure data with AFC represent results are with the PJA device unless explicit mention of SBA is included. Finally, the section 4.3 includes figures of merit for both technologies investigated during these cryogenic experiments.

4.1 Baseline Flow

Fig. 14 shows the lift curves of the baseline flow (with the cutback and without AFC) at various *Re* numbers and for fixed *Ma=0.2*. The largest differences occur both at very low (negative) incidence and close to maximum lift. Moreover the lowest *Re* ($1.5x10^6$) points out a different mechanism for the wing stall (as learned also by other extensive measurements and discussed later). The increase of *Re* results in an

increase in maximum lift and maximum incidence attributed to the reduction of boundary layer losses. The limitation for maximum lift is given by the flow separation downstream the unprotected LE. However the flow separation over a large wing extent occurs *6...10°* later. An example is the result for $Re=2.9x10^6$ where the major lift drop occurs almost *10°* after maximum incidence is reached.

Fig. 15 and Fig. 16 show the results for Mach *Ma=0.16* and *Ma=0.28*. The results at atmospheric conditions and for the lowest Re are prone to deviate from the general trend. For the sake of brevity we will just recall here the identified cause. At low Re the burst of laminar separation bubbles (LSBs), e.g. on the suction side of the TE flap, caused an earlier circulation drop off and consequently lower maximum incidence compared to the results at large Re. An order of three million was identified for the Reynolds number as being a valid cutoff-value. Above this Re number the flow separation downstream the cutout and the general aerodynamic behaviour of the wing showed to avoid the non-linear behavior generated by the LSBs. With respect to the Mach number effects a cross-comparison for Mach between *0.16* and *0.28* is addressed in Fig. 17 for $Re=4.4x10^6$. The increase of incoming Mach number, which results in the increase of compressibility effects causes a slight decrease of lift in the linear range and a drop-off for the maximum angle of attack and corresponding lift. Moreover with the larger Mach a larger portion of the wing suction side is earlier separated and a rapid decrease in lift is measured.

Fig. 18 recalls one result for $Re=5.3x10^6$ and serves as a reference for the discussion of static pressure data measured in the different spanwise sections. As indicated by the circles, four incidences are selected in order to describe the changes over the alpha for the local flow in section DV2, and DV3, i.e. at stations of 25% and 39% of the spanwise extent.

Fig. 19 shows the measured pressure data for the main wing element over the increase of incidence. Up to maximum lift, the larger circulation corresponds to larger suction peaks on wing for all sections. In section 2 (DV2) the wing trailing edge shows an increase in pressure at α_2 together with a drop in flap suction peak (not shown). At α_{max} the change in pressure for the wing of section 2 is understood as a flow recirculation moving upstream, which leads to a large flow separation at α_4 as indicated by the pressure plateau. In this experiment, similar to the CFD, the flow separation occurs inboard of the pylon considering that the pressures of the wing in section 3 (DV3) follow a similar pattern as above described but delayed compared with the pressures from DV2. The pressure data in the outboard sections (not shown) underline the observation that the local flow separation extends between section 2 and section 3, as all three elements of e.g. DV4 show an increase of local circulation with the increase of incidence from α_{max} to α_4. The position and extent of this flow recirculation is later the subject in comparison with the AFC application.

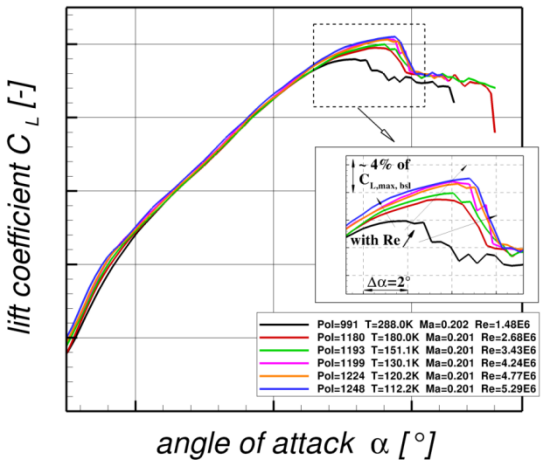

Fig. 14. Reynolds number effect for the lift curves of the baseline configuration with cutback at *Ma=0.2*

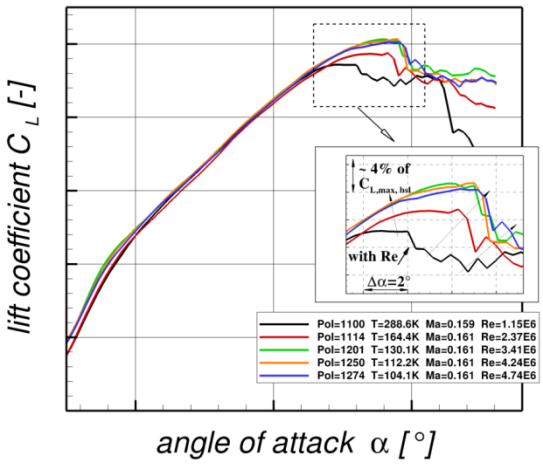

Fig. 15. Reynolds number effect for the lift curves of the baseline configuration with cutback at *Ma=0.16*

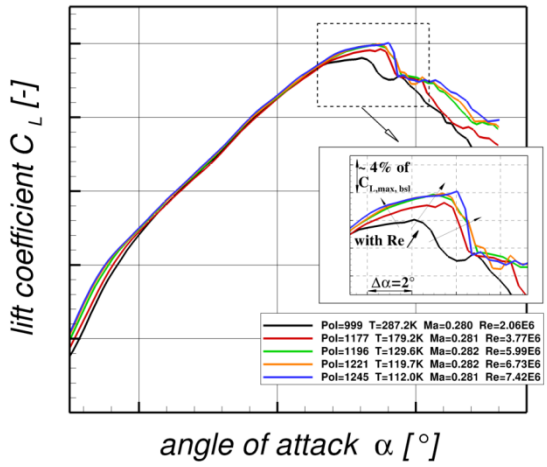

Fig. 16. Reynolds number effect for the lift curves of the baseline configuration with cutback at *Ma=0.28*

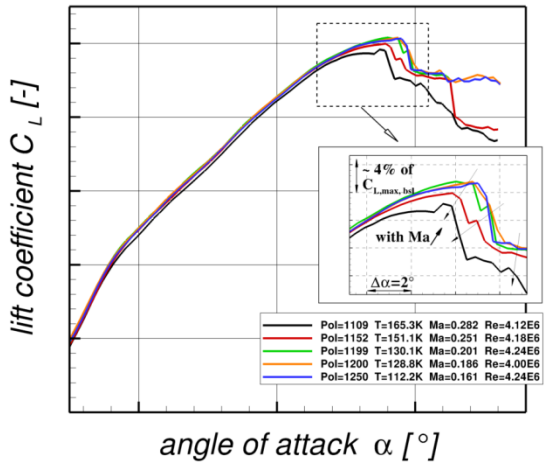

Fig. 17. Mach number effect for the lift curves of the baseline configuration with cutback at $Re \approx 4x10^6$

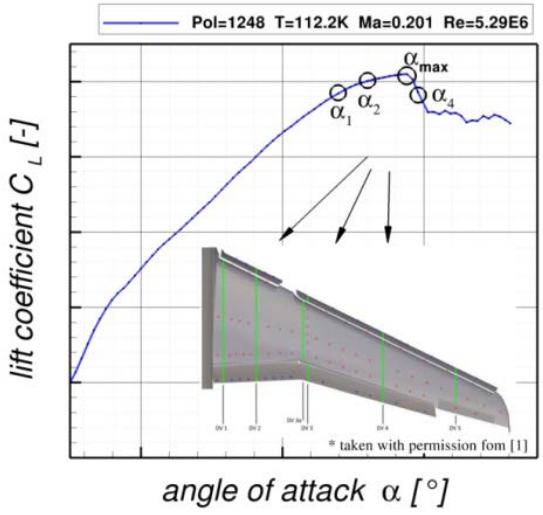

Fig. 18. Lift curve for baseline flow and sketch of the pressure ports positions on the high-lift wing

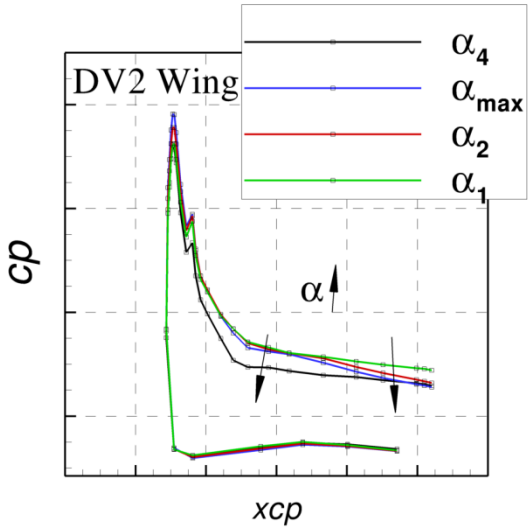

a) η = 25% (DV2)

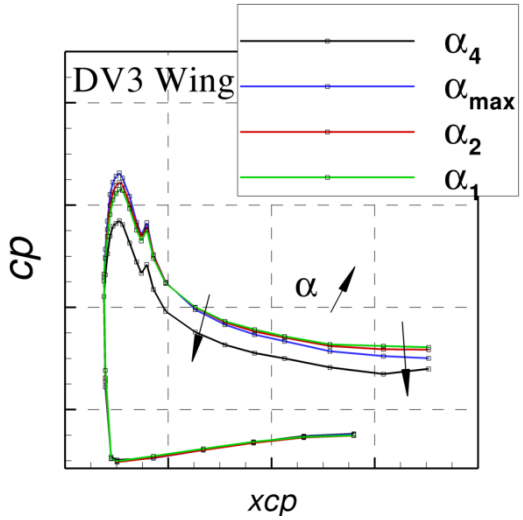

b) η = 39% (DV3)

Fig. 19. Baseline pressure data for wing at two spanwise locations(η)

4.2 With Active Control

Fig. 20 shows the qualitative effect of flow control by tufts visualization. From the tufts videos, images at one large incidence and atmospheric conditions (*T=289K*) are extracted and lines indicate the flow regions of large interest. The baseline flow shows a large flow separation downstream the slat cutout region. With AFC the tufts show a reduced region of flow recirculation with less spanwise extend for local separations. However, both outboard of the actuation region and at the wing trailing edge the tufts indicate large flow unsteadiness and some remaining reversed flow.

a) baseline

b) with AFC (SBA)

Fig. 20. Tufts visualization at *Ma=0.2* and *Re=1.5x10*^{6}

Four lower figures depict the change in lift over the incidence by different actuation blowing momentum coefficients in comparison with the baseline. Fig. 21 and Fig. 22 show results for Mach *Ma=0.16*. Fig. 23 and Fig. 24 show results with flow control for Mach *Ma=0.2*. Fig. 22 and Fig. 23 depict the results for different Mach but for the same *Re=4.2x10*^{6}.

As shown in Fig. 21 the maximum incidence and maximum lift are increased with the increase in blowing momentum coefficient c_μ (triggered with an increase in mass-flow). At $c_{\mu 1}$ the fluidic actuation is mostly neutral compared with the baseline. The larger mass flows show a linear increase of maximum lift over the addition of energy. In Fig. 22 , the *Re=4.2x10*^{6}, case depicts a beneficial effect even for the $c_{\mu 1}$ An extended benefit of the largest $c_{\mu 4}$ below the maximum incidence is observed, i.e. larger lift until aprox. α_{max} +6° with a more stable flow recirculation downstream the cutout.

Fig. 23 and Fig. 24 show the lift alleviation at the Mach of *Ma=0.2*, and only for blowing momentums $c_\mu > c_{\mu 2}$ positive increments by AFC are measured. The trend was expected considering that a lower velocity ratio of the actuation jet relative to the incoming flow typically has no beneficial effect on separation control.

Fig. 26 and Fig. 27 show the pressure data gain in section two (DV2) of the wing as indicators for the local flow behavior with and without AFC. For clarity, Fig. 25 shows first the identification of the angle of attack investigated and used for the cross-comparison. Where α_1, and α_2 remain unchanged, α_{max} and α_4 are case specific.

Fig. 26 shows that the local pressure with and without control remain very similar. The flow breakdown after maximum alpha occurs in the same region. Only larger overall suction peaks indicate a local change. Fig. 27 depicts the comparison of the pressures before and after the fluidic actuation is switched on for a fixed incidence close to maximum lift. The increase in circulation for the wing leading edge suggests a delayed local flow separation, and allows for the upstream element (slat) to have also an increase in local circulation (not shown).

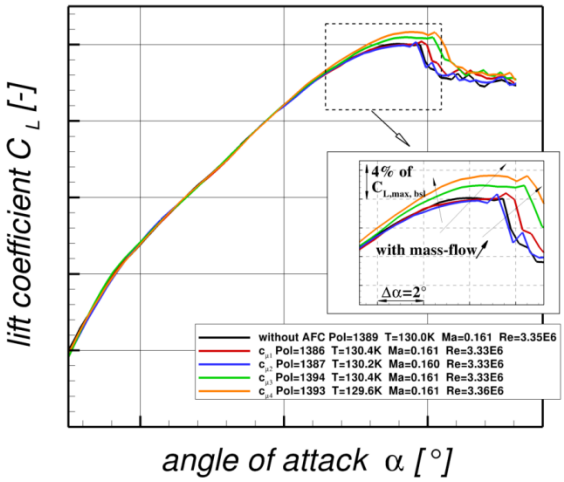

Fig. 21. Lift curve for baseline and with fluidic actuation at *Ma=0.16* and *Re=3.4x10*^{6} ($c_{\mu 1}<c_{\mu 2}<c_{\mu 3}<c_{\mu 4}$)

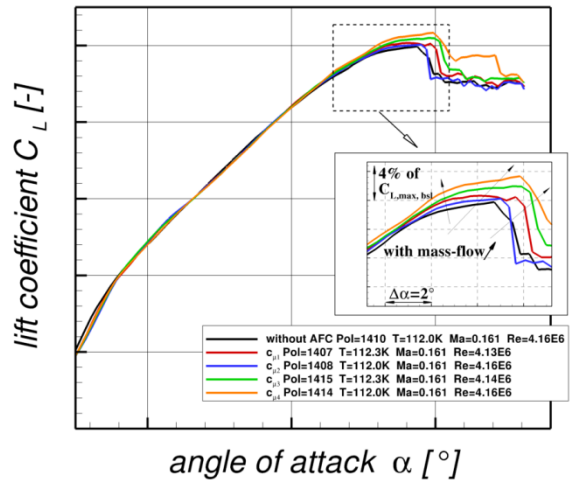

Fig. 22. Lift curve for baseline and with fluidic actuation at *Ma=0.16* and *Re=4.2x10*^{6} ($c_{\mu1}<c_{\mu2}<c_{\mu3}<c_{\mu4}$)

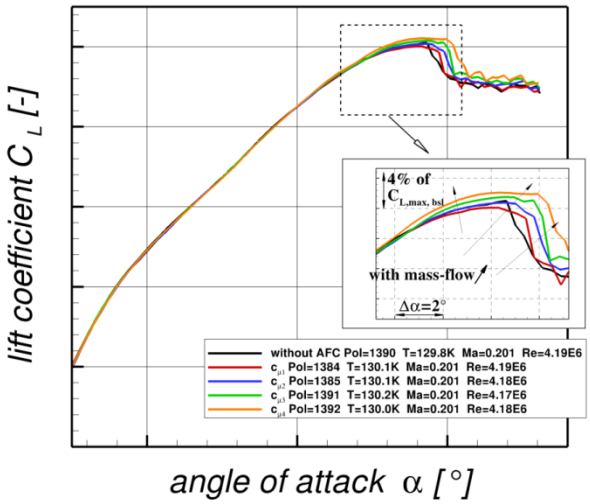

Fig. 23. Lift curve for baseline and with fluidic actuation at *Ma=0.2* and *Re=4.2x10*^{6} ($c_{\mu1}<c_{\mu2}<c_{\mu3}<c_{\mu4}$)

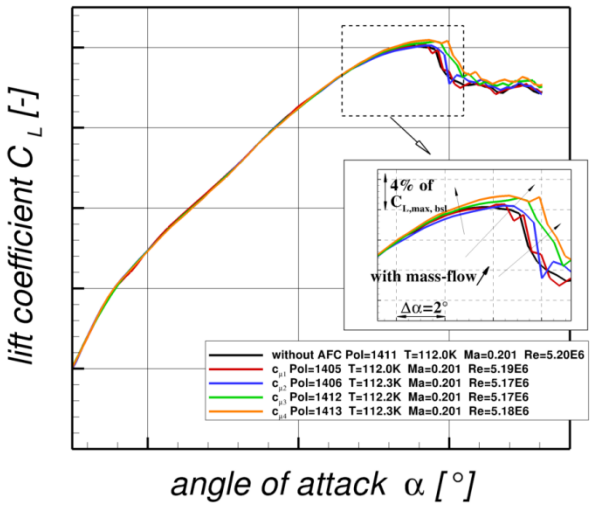

Fig. 24. Lift curve for baseline and with fluidic actuation at *Ma=0.2* and *Re=5.2x10*^{6} ($c_{\mu1}<c_{\mu2}<c_{\mu3}<c_{\mu4}$)

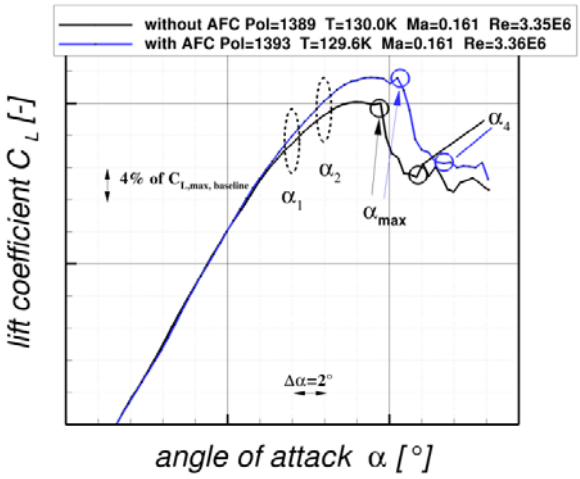

Fig. 25. Lift curve for baseline and with fluidic actuation at *Ma=0.16* and *Re=3.42x10*^{6} with identification of angles $\alpha_1 \ldots \alpha_4$

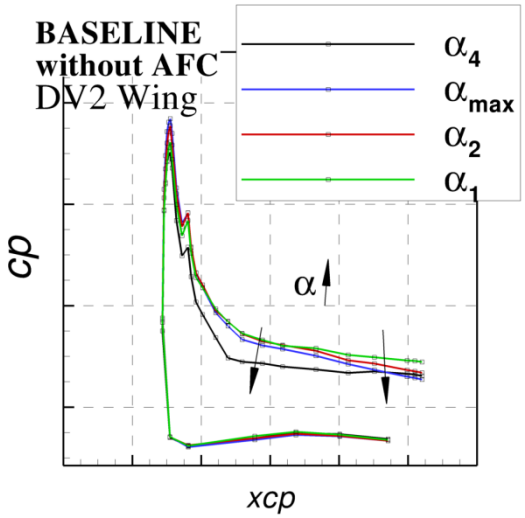

a) without AFC

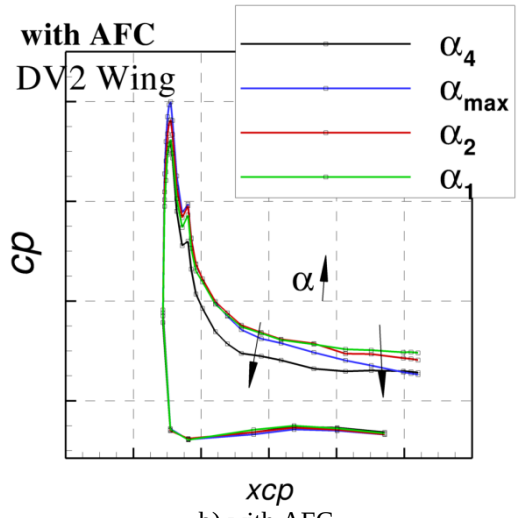

b) with AFC

Fig. 26. Pressure data for wing at one spanwise location (η=25%) with increasing incidence (*Ma=0.16*, *Re=3.4x10*^{6})

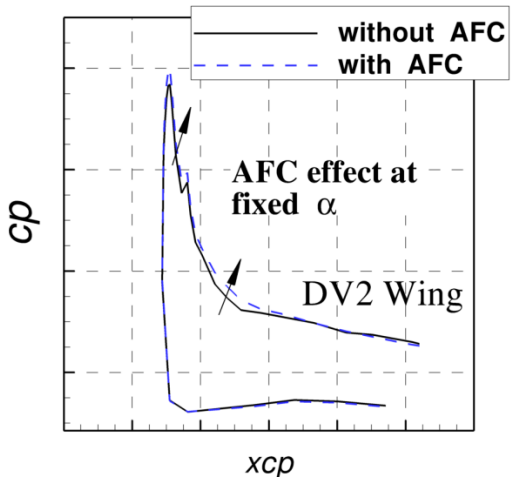

Fig. 27. Pressure data for wing at η=25% for fixed and large α (*Ma=0.16*, *Re=3.4x10*^{6})

4.3 Figures of Merit

Fig. 28 summarizes the maximum incidence increments measured for two Mach numbers and for both actuation systems. On the left side of the figure, the results are depicted for the pulsed jet actuators (PJA) and on the right side for the steady tangential blowing actuation (SBA). Please note on the left side the lower blowing momentum coefficients compared to the right graphs resulting by applying a dynamic actuation through a smaller exit surface. For both *Ma=0.16* and *Ma=0.2* increments of *1°* and above are shown with the PJA- and SBA-systems. While for low c_μ the PJA shows in several cases a reduction of maximum AoA, with the increase of energy addition there is an increase in incidence and most measured values show gains of $\Delta\alpha >= 1°$. With the SBA the incidence gain is mostly larger the larger the blowing momentum coefficient for *Ma=0.2*. At low speed, *Ma=0.16*, the change in maximum incidence due to the steady tangential blowing shows no direct dependency on the c_μ, but perhaps influenced by other parameters, e.g. the *Re* number.

Fig. 29 depicts the measured maximum lift values for the baselines and with PJA at two mass flows V_{N1} and V_{N2}. The shaded areas in grey and in magenta indicate the maximum lift gains by AFC. At *Ma=0.16* the lift increments increase with the larger *Re* but decrease for the lower *Re*. At *Ma=0.2* the maximum gain is reached for *Re=3.4x10*^{6} and after a drop at *Re=4.2 x10*^{6}, a further increase of maximum lift is measured at *Re=5.3x10*^{6}. Nevertheless, a general *2%* increase of maximum lift for the V_{N2} compared with the baseline is shown for a large range of *Re*.

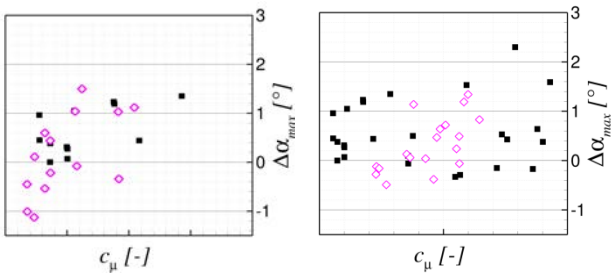

Fig. 28. Increments for maximum AoA at Re > *3x10*^{6} due to the fluidic actuation (left: PJA) and steady blowing (right: SBA)

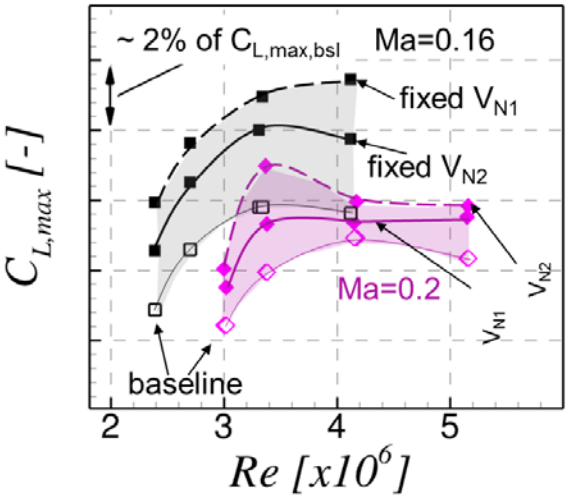

Fig. 29. Reynolds effects on maximum lift with and without the fluidic actuation (PJA) at *Ma=0.16* and *Ma=0.2*

Fig. 30 depicts the measured maximum lift values for the baselines and with SBA at a fixed mass flow. Similarly, the shaded areas in grey and in magenta indicate the maximum lift gains by AFC. At *Ma=0.16* the lift increments remain mostly constant over the *Re* number. The maximum lift over the *Re* variation is reached slightly earlier with AFC compared with the baseline flow. However if one excludes the low *Re* results dependent on effects such as local LSBs, the AFC gain is quasi-constant for *Re=3…5 x10*^{6}. At *Ma=0.2* the maximum gains are reached for *Re>4.5x10*^{6}. In general *1.5%* increase of maximum lift compared with the baseline is shown for a large range of *Re* at the *Ma=0.2*.

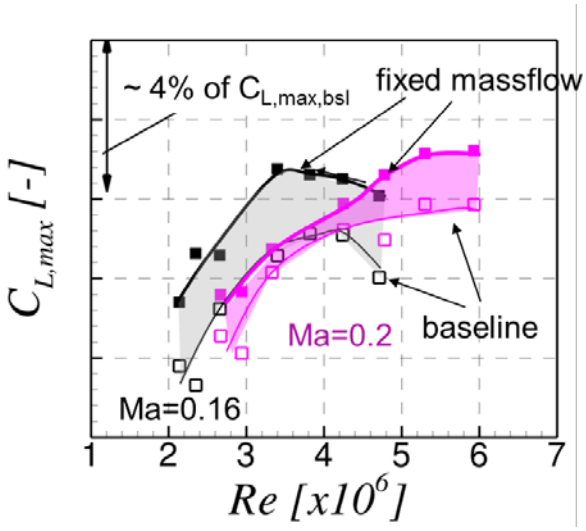

Fig. 30. Reynolds effects on maximum lift with and without the steady blowing actuation (SBA) at *Ma=0.16* and *Ma=0.2*

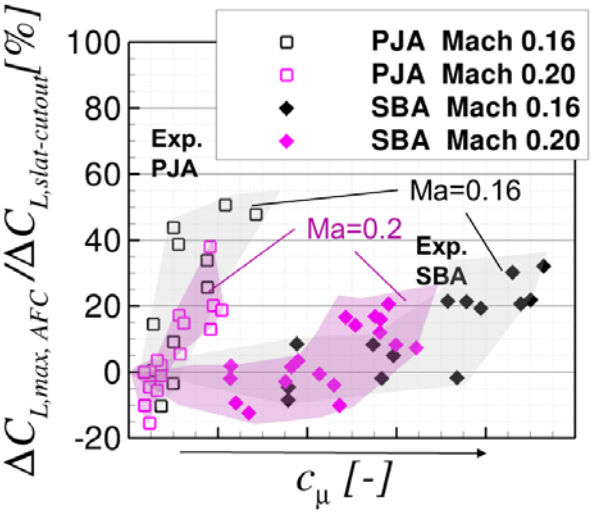

Fig. 31. Relative increments of maximum lift over the actuation blowing momentum coefficient for PJA and SBA at *Ma=0.16* and *Ma=0.2* (here CleanSky2 is compared with DLR reference data for the baseline without slat cutout)

Fig. 31 shows the relative maximum lift increments for the two actuation systems. The gain by flow control $\Delta C_{Lmax,AFC}$ is computed as a difference between maximum lift with control and maximum lift with the unprotected leading edge, or so-called cutout and the resulting inboard slat reduction. This gain is shown relative to the lift loss generated by the cutout, i.e. relative to the $\Delta C_{Lmax,slat\text{-}cutout}$ which is a difference between reference maximum lift of this configuration at landing and the here measured maximum lift of the baseline with cutout. Only results for $Re > 3x10^6$ are shown. First the measured range for c_μ differs between the two technologies. Second, the general increase in maximum lift with the blowing momentum is steeper with the PJA than with the SBA, i.e. lower values for c_μ are required to reach the same target by means of lift increments. Third, for the lower Mach, *Ma=0.16*, a recovery in the order of 50% is measured when applying the PJA. Finally, both technologies deliver increments in the order of *20%* and above while $c_\mu < 1x10^{-2}$ for both Mach numbers relevant for low speed flight conditions.

The level of recovery is good, considering the targets for the AFC application. For ATRA a/c the *Ma=0.2* corresponds to the approach speed with the aircraft at maximum landing weight (MLW) and at standard conditions for pressure and temperature. This speed is used for gaining also the aerodynamic reference polars by experiments and tunnel simulations. Nevertheless, the stall speed is less by a factor of *1.23*. For our application, close to the wing stall, the a/c speeds of *Ma=0.12* to *Ma=0.16* can become important for the flow separation control.

5. Conclusions

The study for AFC towards the application at the pylon wing junction was depicted starting with early CFD findings and continuing with detailed experimental results at high-*Re* numbers. These results can be summarized as:

- the fluidic actuation can delay the wing stall when applied in the region of the unprotected wing leading edge.
- high *Re* testing with and without AFC increased the knowledge base for this LE application. Testing at least at $Re > 3x10^6$ is learned to be a must with this configuration towards a possible flight test.
- the limitation for the maximum lift of this wing is characterized by local separation downstream the unprotected leading edge inbord of the under-the wing mounted pylon. The stall starts mostly at the wing trailing edge. This behavior remains valid both with and without flow control.
- lift recovery by AFC compared to the impact of a cutout on the high-lift configuration can be as high as *50%* at

moderate Mach (*Ma=0.16*). For the large Mach (*Ma≈0.2*) the maximum lift gain is in the order on *20%* with low blowing momentum coefficients c_μ *<1x10*$^{-2}$.

- the joint effort of CFD and wind tunnel testing remains a strong approach to push this AFC technology.
- a second test in DNW-KKK is planned for the autumn 2018 to investigate improved actuation systems towards the application of local separation control. The decision regarding a flight test with a short range a/c will consider these final wind tunnel data.

6. Acknowledgments

The work is performed in strong collaboration between the partners Airbus GmbH, German Aerospace Center (DLR), NAVASTO GmbH, Netherlands Aerospace Centre (NLR) and the cryogenic facility DNW-KKK of the German Dutch Wind Tunnels (DNW). The authors would like to thank Justin Dorneanu (NLR), Fabian Lange (DLR), Carsten Lenfers (DNW), Jakob Lohse (Navasto), Stefan Melber-Wilkending (DLR), and Ralf Rudnik (DLR) for their contributions. The work and the research leading to these results have received funding from the Clean Sky 2 Joint Undertaking under the European Union's Horizon 2020 research and innovation programme under grant agreement No CS2- LPAGAM- 2014-2015-01 [13].

References

[1] Lange Fabian: Aerodynamic Optimization of an UHBR Engine Position on a Representative Short Range Aircraft Configuration at Cruise Flight Conditions. AIAA Paper 2018-3811.

[2] Lengers Matthias.: Industrial Assessment of Overall Aircraft Driven Local Active Flow Control, *ICAS*, 2014.

[3] Fricke Sebastian, Ciobaca Vlad, Kröhnert Anna, Wild Jochen, and Blesbois Olivier.: Active Flow Control Applied at the Engine-Wing Junction. In proceeding of *CEAS* 2015.

[4] Meyer Michael, and Wildschek Andreas.: Design and Validation of Active Flow Separation Control at the Wing/Engine Junction. In proceeding of *ECCOMAS* 2016.

[5] Bauer Matthias, Lohse Jakob, Haucke Frank, and Nitsche Wolfgang: High-lift performance investigation of a two-element configuration with a two-stage actuator system, *AIAA J*. 2014, 52, 1307–1313.

[6] Cord-Christian Rossow: *Handbuch der Luftfahrzeugtechnik*. ISBN: 978-3-446-42341-1, 2014.

[7] Lachmann G.V.. *Boundary Layer and Flow Control: Its Principles and Applications*. Pergamonn Press,London, 1961.

[8] Joslin R. and Miller D. *Fundamentals and Applications of Modern Flow Control*. AIAA, Inc., Reston, Virginia, Vol. 231, Progress in Astronautics and Aeronautics, 2009.

[9] Smith A.M.O.. High-Lift Aerodynamics. Journal of Aircraft, 12:501–530, 1975.

[10] Ciobaca Vlad, Wild Jochen, Bauer Matthias, Grund Thomas, Huehne C.-P., Scholz Peter, Stefes Bruno. Wind Tunnel Experiments with Active Flow Control for an Outer Wing Model, AIAA Paper 2015-2728.

[11] Rosenblum Jean-Pierre, Prachar Ales, Peng Shia-Hui, Wallin Stefan, Eliasson Peter, Iannielli Pierluigi, Ciobaca Vlad, Wild Jochen, Gervois Jean-Luc-Hartrais, Costes M.. Active Flow Separation Control at the Outer Wing. In proceedings of CEAS 2017.

[12] Amiryants Genadi, Schlösser Philipp, Bauer Matthias, Wild Jochen, Weigel Perez, Bardet Michael, Gebhardt Anna, Ciobaca Vlad. Full-Scale Wind-Tunnel Test of Active Flow Control at the Wing/Pylon/Engine Junction. In proceeding of CEAS 2017.

[13] www.cleansky.eu

[14] Ciobaca Vlad. *Validation of Numerical Simulations for Separation Control on High-Lift Configurations*. Deutsches Zentrum für Luft- und Raumfahrt, FB 2014-11, TU Berlin Dissertation 2014.

[15] Gebhardt Anna and Kirz Jochen. Numerical investigation of slot variations on the efficiency of tangential blowing at a vertical tailplane with infinite span J. CEAS Aeronaut J(2018) 9:195.

[16] Rudnik Ralf, Schwetzler Detlev. High lift INflight VAlidation (HINVA) - Overview about the 2nd Flight Test Campaign. AIAA Paper 2016-0041.

[17] Bier Niko, Rudnik Ralf, Quest Jürgen and Rechlin Alexander.: Stall Behavior of the HINVA KH-A320-HA Highlift Model in ETW, *AIAA Paper* 2015-1226.

[18] Casper Marcus, Scholz Peter, Radespiel Rolf, Wild Jochen, and Ciobaca Vlad. Separation control on a High-Lift Airfoil using Vortex Generator Jets at High Reynolds numbers. AIAA Paper 2011-3442, 2011.

[19] Zhai Junnai and Vree Amand, Advancement of Half-Model Testing at DNW-KKK in Proceedings of 11th International Symposium on Strain-Gauge Balances, Cologne, Germany 2018.

Copyright Statement